Chirped coherent anti-Stokes Raman scattering as a high-spectral- and spatial-resolution microscopy

Robert M. Onorato,[1] Naoki Muraki,[1,2] Kelly P. Knutsen,[1] and Richard J. Saykally[1,*]

[1]*Department of Chemistry, University of California, Berkeley, California 94720, USA*
[2]*Materials Science Laboratory, Toray Research Center, Inc., 3-3-7 Sonoyama, Otsu, Shiga, 520-8567, Japan*
**Corresponding author: saykally@berkeley.edu*

Received June 21, 2007; revised August 27, 2007; accepted August 29, 2007;
posted August 31, 2007 (Doc. ID 84419); published September 27, 2007

Coherent anti-Stokes Raman scattering (CARS) microscopy is a promising tool for chemically selective imaging based on molecular vibrations. While CARS is currently used as a biological imaging tool, many variations are still being developed, perhaps the most important being multiplex CARS microscopy. Multiplex CARS has the advantage of comparing images based on different molecular vibrations without changing the excitation wavelengths. Here we demonstrate both high-spectral- and spatial-resolution multiplex CARS imaging of polymer films, using a simple scheme for chirped CARS with a spectral bandwidth of 300 cm^{-1}.

OCIS codes: 110.0180, 160.5470, 180.5810, 190.4380, 300.6230.

Coherent anti-Stokes Raman scattering (CARS) is rapidly evolving into an effective chemically selective imaging technique, exploiting molecular vibrations as endogenous chromophores. CARS is a third-order nonlinear process that achieves chemical specificity through a vibrational coherence at the frequency $\omega_p - \omega_s$ driven by two laser pulses at different frequencies, the pump pulse (ω_p) and the Stokes pulse (ω_s). The resulting CARS signal is generated at the frequency $2\omega_p - \omega_s$ by the probe pulse interacting with the vibrational coherence. Many different variations of CARS have been developed to minimize the nonresonant signal that is inherent to any nonlinear optical process, including epidetection [1], polarization control [2,3], and interferometry [4–7].

One of the current challenges in CARS microscopy is the development of an effective multiplex CARS imaging technique. Multiplex CARS is achieved by exciting a range of frequencies determined by the energy difference $\omega_p - \omega_s$ and is therefore able to probe multiple molecular vibrations simultaneously. This can be done by using a broadband Stokes pulse, as shown in Fig. 1. There are various methods currently being used to generate multiplex CARS signals, all of which utilize femtosecond lasers: synchronizing femtosecond and picosecond laser pulses in time [8], using a photonic crystal fiber to generate a continuum that is used as the Stokes pulse [9], using a pulse shaper [5,10], and chirping the probe pulse [11]. The latter three utilize a single laser pulse to generate both the degenerate pump–probe pulse and the Stokes pulse, transcending the complication of synchronizing two lasers in time.

In chirped CARS (c-CARS), the degenerate pump–probe pulse is chirped and then overlapped in time with a transform-limited broadband femtosecond Stokes pulse; both pulses are generated from the same seed pulse. The overlap of the pump and Stokes pulses resonantly excites vibrational coherences at the frequencies $\omega_p - \omega_s$ within a bandwidth proportional to that of the Stokes pulse. These vibrational coherences are probed by the chirped pulse, generating the c-CARS signal. In the limiting case that the dephasing time of the coherence is of the order of the temporal pulse width of the Stokes pulse, the spectral resolution is determined by multiplying the chirp rate of the pump–probe pulse and the temporal width of the Stokes pulse.

However, when the dephasing time of the vibrational coherence, normally hundreds of femtoseconds to picoseconds, is of the order of or larger than one half the temporal width of the chirped pulse (about 5 ps for all spectra and images in this Letter), there will be c-CARS signal generated during and after the temporal overlap of the pump–probe and Stokes pulses. Since the pulse is negatively chirped, this creates a distorted line shape on the low-frequency side of each peak, which appears as an exponential decay of the vibrational mode convoluted with a ringing pattern due to the interaction of multiple electric fields and their phases evolving in time.

This lifetime is generally much shorter for nonliquid samples, such as the polymer samples described in this Letter, and in this case the effect is insignifi-

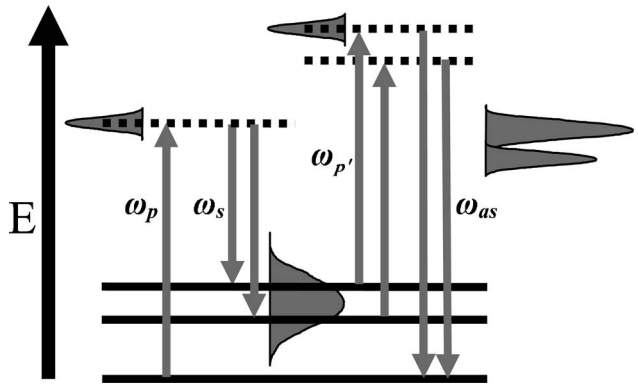

Fig. 1. Multiplex CARS energy level diagram. Narrowbandwidth pump and probe pulses mix with a broadband Stokes pulse, yielding a high-resolution anti-Stokes signal.

0146-9592/07/192858-3/$15.00

cant. In cases where the effect is significant it can be minimized by decreasing the chirp rate, resulting in a temporally longer pulse and a decrease in the extent of the interaction between the dephasing vibrational coherence and the chirped pulse.

Spectra exhibiting 10 cm^{-1} spectral resolution with a spectral bandwidth of 300 cm^{-1} were previously reported with calculations from a simple model supporting the analysis [12]. Previous c-CARS imaging has been demonstrated with polystyrene beads [12]; however, this did not demonstrate the multiplex capabilities of c-CARS imaging. In this Letter, multiplex imaging is demonstrated with c-CARS for the first time to our knowledge, using a phase-separated polymer film blend of polystyrene (PS) and poly(vinyl methyl ether) (PVME). C-CARS lateral spatial resolution approaching the theoretical limit is also shown.

Femtosecond pulses are generated in a home-built Ti:sapphire oscillator, which seeds a regenerative amplifier (Spectra Physics, Spitfire). The amplified output is split; approximately 5% is used to generate the chirped pulses with a pair of diffraction gratings, while the remaining output is used to pump an optical parametric amplifier (Light Conversion, TOPAS), providing tunable infrared light, which is doubled with a BBO crystal. The chirped and doubled idler pulses are spatially and temporally overlapped and focused onto the sample by a 1.2 NA objective (Olympus, UPLSAPO 60XW) and collected by a matched objective. The CARS signal is dispersed by a spectrograph (Acton Research, SpectraPro 300i) and collected with a CCD (Roper Scientific, Spec10B-LN2) for spectra and with a photomultiplier tube (PMT) for images. The bandwidth of the signal collected by the PMT can be controlled by the exit slit width of the spectrograph.

Grains of PS (M_n=140,000, M_w=230,000, Sigma-Aldrich) and 50 wt. % PVME toluene solution (SP2 Inc.) were used to prepare thin films (~15 μm thick) of a 1:1 blend from 10 wt. % toluene solutions by drop casting on glass slides. The film was heated in a vacuum oven at 50°C for at least three days. The homogeneous film has a lower critical solution temperature, and hence the phase separation into PS- and PVME-rich domains was thermally induced by heating at a temperature above the binodal points, 128°C, from 60 to 240 s, corresponding to domain sizes of approximately 0.1–10 μm.

C-CARS spectra of the PVME- and PS-rich domains of a film that was heated for 240 s are shown in Fig. 2(a). The PVME-rich domain spectrum is dominated by the asymmetric aliphatic C—H stretch near 2900 cm^{-1}. The two smaller features are the symmetric C—H stretch near 2850 cm^{-1} and an aromatic C—H stretch near 3050 cm^{-1}, which is due to the small amount of PS in the PVME-rich domain. The PS-rich domain spectrum exhibits the same C—H vibrations, but with different intensities. The aromatic C—H signal and the asymmetric aliphatic C—H signal are of similar intensities and are both more intense than the asymmetric aliphatic C—H signal of the PVME-rich region.

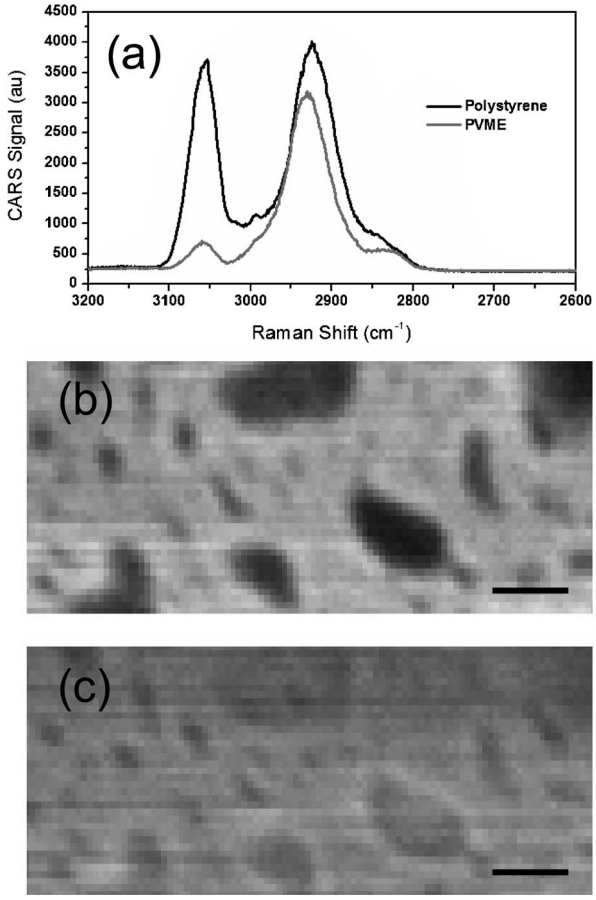

Fig. 2. (a) C-CARS spectra of PS- and PVME-rich polymer film domains. The peaks at 3050, 2900, and 2850 cm^{-1} are the aromatic C—H stretching mode and the asymmetric and symmetric aliphatic C—H stretching modes, respectively. C-CARS images utilizing the aromatic (b) and aliphatic (c) C—H stretching modes. The scale bars are 3 μm.

The image in Fig. 2(b) is a c-CARS image collecting the aromatic C—H stretching signal of a polymer film, showing a strong contrast between the PS- and PVME-rich regions. The light regions correspond to the aromatic c-CARS signal of the PS-rich domains, and the dark regions correspond to the PVME-rich regions that produce relatively little c-CARS signal in the aromatic spectral region. Figure 2(c) is an image of the same polymer film region taken by collecting the asymmetric aliphatic signal. This image shows a much weaker contrast. The PS-rich domains exhibit stronger signal than the PVME-rich domains, but the difference between the two domains is much less significant, since both regions provide a strong aliphatic C—H response.

The image in Fig. 3(a) shows clearly resolved 480 nm PS beads on a glass slide. This image was acquired by collecting the aromatic C—H signal and has a signal-to-noise ratio of approximately 11:1. Line scans of this image, Fig. 3(b), show that two adjacent PS beads are resolved by using c-CARS. The theoretical lateral resolution was calculated by using the method of Cheng *et al.* [13] to be 350 nm. Figures 4(a) and 4(b) show an aromatic C—H stretching region image and line scan, respectively, of a PS/PVME polymer film that was heated for 60 s. The error bars

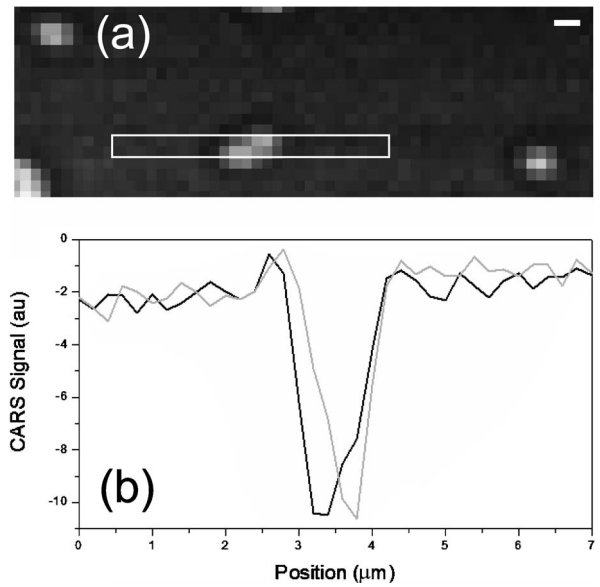

Fig. 3. (a) C-CARS image of 480 nm PS beads. The scale bar is 500 nm. (b) C-CARS line scans of the region in (a) outlined in white, showing that the peaks due to two adjacent PS beads, are clearly resolved.

in the line scan represent the noise in the c-CARS signal of a PVME-rich domain of Fig. 2(b) and are therefore an upper limit on the noise level. Since pixel-to-pixel signal variations are often much greater than the error bars, it is clear that there are pixel-to-pixel signal variations due to the domain structures of the polymer films. This demonstrates that the achieved c-CARS spatial resolution is consistent with the calculated resolution.

We have demonstrated the multiplex chemically selective imaging ability of c-CARS as well as the ability of this technique to achieve high spatial resolution. While a number of c-CARS techniques have demonstrated imaging on relatively simple systems, to our knowledge there has yet to be a multiplex CARS study on a more complicated system wherein the sample is not composed primarily of the probed endogenous chromophore. The difficulty in multiplex CARS imaging arises from the balance between the decreased signal-to-noise ratio relative to single-frequency CARS and remaining below the sample damage threshold. The CARS intensity is proportional to the Stokes pulse intensity, and since multiplex CARS disperses the usable pulse intensity over a broad range of frequencies, there is a decrease in the signal-to-noise ratio at each frequency for multiplex CARS relative to single-frequency CARS at a given Stokes intensity. The intensity at each frequency could be increased by an overall increase in the Stokes pulse intensity, but this can lead to significant photodamage of the sample. Fu *et al.* [14] provide a detailed account of CARS photodamage using picosecond lasers. The mechanisms of photodamage for multiplex CARS differ because of the use of femtosecond pulses [15]. The challenge of multiplex CARS remains that of achieving a sufficiently high signal-to-noise ratio while the intensity of the incident pulses remains below the damage threshold.

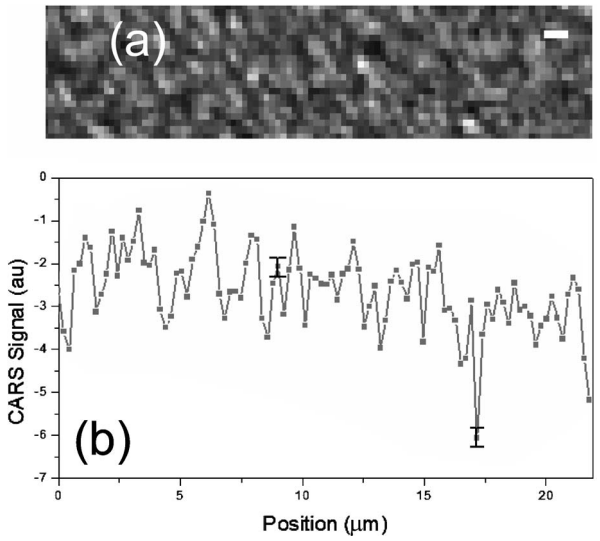

Fig. 4. (a) Aromatic C—H stretching region c-CARS image of PS- and PVME-rich polymer film domains. Pixel size 220 nm. The scale bar in the upper right is 1 μm. (b) Representative line scan of the C-CARS signal in (a). The error bars represent the noise in the c-CARS signal of a PVME-rich domain of Fig. 2(b).

This work was funded by the NASA Sample Return Laboratory Instruments and Data Analysis Program and the National Science Foundation under grant 404571.

References

1. J. X. Cheng, A. Volkmer, L. D. Book, and X. S. Xie, J. Phys. Chem. B **105**, 1277 (2001).
2. J. J. Song, G. L. Eesley, and M. D. Levenson, Appl. Phys. Lett. **29**, 567 (1976).
3. J. X. Cheng, L. D. Book, and X. S. Xie, Opt. Lett. **26**, 1341 (2001).
4. C. Vinegoni, J. S. Bredfeldt, D. L. Marks, and S. A. Boppart, Opt. Express **12**, 331 (2004).
5. S. H. Lim, A. G. Caster, and S. R. Leone, Phys. Rev. A **72**, (2005).
6. E. O. Potma, C. L. Evans, and X. S. Xie, Opt. Lett. **31**, 241 (2006).
7. T. W. Kee, H. X. Zhao, and M. T. Cicerone, Opt. Express **14**, 3631 (2006).
8. M. Muller and J. M. Schins, J. Phys. Chem. B **106**, 3715 (2002).
9. T. W. Kee and M. T. Cicerone, Opt. Lett. **29**, 2701 (2004).
10. D. Oron, N. Dudovich, D. Yelin, and Y. Silberberg, Phys. Rev. Lett. **88**, 063004 (2002).
11. K. P. Knutsen, J. C. Johnson, A. E. Miller, P. B. Petersen, and R. J. Saykally, Chem. Phys. Lett. **387**, 436 (2004).
12. K. P. Knutsen, B. M. Messer, R. M. Onorato, and R. J. Saykally, J. Phys. Chem. B **110**, 5854 (2006).
13. J. X. Cheng, A. Volkmer, and X. S. Xie, J. Opt. Soc. Am. B **19**, 1363 (2002).
14. Y. Fu, H. F. Wang, R. Y. Shi, and J. X. Cheng, Opt. Express **14**, 3942 (2006).
15. H. J. Koester, D. Baur, R. Uhl, and S. W. Hell, Biophys. J. **77**, 2226 (1999).